648 *Chem. Mater.* **2010,** *22,* 648–659
DOI:10.1021/cm902195j

CHEMISTRY OF MATERIALS
Review

Nanostructured Thermoelectrics: The New Paradigm?[†]

Mercouri G. Kanatzidis*

Department of Chemistry, Northwestern University, Evanston, Illinois 60208, and Materials Science Division, Argonne National Laboratory, Argonne, Illinois 60439

Received July 18, 2009. Revised Manuscript Received September 6, 2009

This review discusses recent developments and current research in bulk thermoelectric materials in which nanostructuring is a key aspect affecting thermoelectric performance. Systems based on PbTe, $AgPb_mSbTe_{2+m}$, $NaPb_mSbTe_{2+m}$, Bi_2Te_3, and Si are given particular emphasis. To date the dramatic enhancements in figure of merit in bulk nanostructured materials come from very large reductions in lattice thermal conductivity rather than improvement in power factors. A discussion of future possible strategies is aimed at enhancing the thermoelectric figure of merit of these materials.

Introduction

When it comes to thermoelectric (TE) devices it is all about increasing the figure of merit $ZT = (S^2\sigma/\kappa)T$ where T is the temperature, S is the Seebeck coefficient, σ is the electronic conductivity, and κ is the thermal conductivity. ZT determines the fraction of the Carnot efficiency that can be theoretically attained by a thermoelectric material.[1] The quantity $S^2\sigma$ is called the power factor (PF) and is the key to achieving high performance. A large PF means that a large voltage and a high current are generated during power generation. The thermal conductivity $\kappa = \kappa_{el} + \kappa_{latt}$, where κ_{latt} and κ_{el} are the lattice and carrier thermal conductivity, respectively. The first generation of bulk thermoelectrics was developed over four decades ago with ZT of ~0.8−1.0, and devices made of them can operate at ~5−6% conversion efficiency. Out of a wide variety of research approaches to increase ZT, one has emerged recently which has led to nearly doubling of the ZT at high temperatures and has now given rise to the second generation of bulk thermoelectric materials with ZT ranging from 1.3 to 1.7. This approach is the optimization of existing materials using nanoscale inclusions and compositional inhomogeneities, which can dramatically suppress the lattice thermal conductivity. The new materials are expected to produce power generation devices with conversion efficiencies of 11−15%. Continued progress is expected to raise the ZT by a factor of 2, and depending on ΔT, the predicted efficiency increases to over 20%, a highly exciting prospect which will surely have a large impact in the energy production and conservation fields.

Thin film superlattice structures such as those of PbTe−PbSe (grown with molecular beam epitaxy, MBE) and Bi_2Te_3−Sb_2Te_3 (grown with chemical vapor deposition) with nanoscale features were the first to claim extremely low lattice thermal conductivities.[2,3] These reports motivated the investigation of additional systems and particularly bulk materials because of the belief that the application of the costly and delicate superlattice structures in real world devices is unrealistic. It is interesting to note that the extremely low lattice thermal conductivities claimed for these materials were not experimentally measured but deduced indirectly from other measurements. A recent report on actual lattice thermal conductivity measurements of MBE grown PbTe−PbSe superlattice structures found that this property is not as low as originally claimed.[4] This new information casts doubt on the very small magnitude of the thermal conductivities of thin films and calls for a reinvestigation. Despite this uncertainty, the investigations of bulk materials that followed the thin film reports did produce systems with extremely low lattice thermal conductivities and correspondingly high ZT.[5,6]

Here we review recent progress in enhancing the performance of bulk thermoelectric materials using the nanostructuring approach. The power of this approach is now more fully appreciated, and it is fair to consider it a new paradigm in designing and optimizing thermoelectric materials.

Reducing Thermal Conductivity

Historically, a successful strategy to increase ZT has been to modify an already promising compound by introducing point defects through the synthesis of isostructural solid solution alloys. The solid solutions feature atomic mass fluctuations in the crystal lattice (i.e., disorder) which causes strong phonon scattering and generally can lead to significantly lower thermal conductivity. The canonical example of this is the Bi_2Te_3 system for which the $Bi_{2-x}Sb_xTe_3$ and $Bi_2Te_{3-x}Se_x$ solid solutions are superior to the parent compound in thermoelectric performance.[7,8] The solid solution alloying between two isostructural phases (e.g., A and B) results in a minimum of thermal conductivity at some composition

[†] Accepted as part of the 2010 "Materials Chemistry of Energy Conversion Special Issue".

Published on Web 10/07/2009

$A_{1-x}B_x$ which is called the "alloy limit". Often, however, solid solution alloying can lead to deterioration in electronic performance (e.g., mobility), and an overall gain in ZT cannot be realized. This is the case between the PbTe and $(PbTe)_{1-x}(PbSe)_x$ systems. In the past it was believed that the "alloy limit" was the lowest that could be achieved in a A−B material system.

Slack proposed the "phonon glass electron crystal" (PGEC) idea as a means to achieve record low lattice thermal conductivities without a deterioration in electronic performance.[9] A PGEC material features cages or tunnels in its crystal structure inside which reside massive atoms that are small enough relative to the cage to "rattle". "Rattling" frequencies are low and produce phonon damping that can result in dramatic reduction of the lattice thermal conductivity. In the PGEC picture a glass-like thermal conductivity can in principle coexist with charge carriers of high mobility. The PGEC approach has stimulated significant new research and has led to marked increases in ZT for several compounds such as the clathrates.[10−21] To date, it has not been proven that a PGEC material exists. In most cases of purported PGEC materials, other factors coexist which also account for the observed reduction in thermal conductivity.

Finally, major reductions in the thermal conductivity have come through nanostructuring of bulk materials especially from "bottom up" approaches. It has now been shown that thermal conductivity values well below the "alloy limit" can be achieved. For example, several synthetic techniques have been applied to prepare nanostructured PbTe, with exceptional reductions in the thermal conductivity. Specific examples of dramatic reduction in PbTe derivatives will be discussed below. At this stage two major types of bulk nanostructured materials are emerging, (a) materials with self-formed inhomogeneities on the nanoscale driven by phase segregation phenomena such as spinodal decomposition and nucleation and growth and (b) materials which have been processed (e.g., ground) so they are broken up into nanocrystalline pieces which then are sintered or pressed into bulk objects. Enhanced thermoelectric performance compared to a corresponding non-nanostructured material has been achieved in both types.

Bulk Nanostructured Thermoelectrics

Numerous thermoelectric materials systems have been developed and reviewed previously.[6,22−31] Here we focus on bulk thermoelectric materials and the new thinking regarding the design and optimization of thermoelectric materials. Nanostructuring in bulk materials was discovered first in the system $AgPb_mSbTe_{2+m}$ (LAST-*m*). This is an inherent property of this system and was subsequently predicted to exist in related systems such as $NaPb_mSbTe_{2+m}$ (SALT-*m*) and KPb_mSbTe_{2+m} (PLAT-*m*).

PbTe

Before we discuss the nanostructured PbTe materials we will briefly review the neat PbTe system and its solid solutions which are believed to be homogeneous with no reported evidence of nanostructuring. These systems are the benchmarks against which to compare the nanostructured materials. PbTe has been the premiere thermoelectric material for midrange temperature (600−800 K) applications. It crystallizes in the NaCl crystal structure with Pb atoms occupying the cation and Te forming the anionic lattice. A band gap of 0.32 eV allows the system to be optimized for power generation applications and can be doped either n- or p-type with appropriate dopants. The maximum ZT for PbTe has been reported to be 0.8−1.0 at ∼650 K. The thermoelectric properties and electron transport of PbTe are reasonably well understood and have been reviewed previously.[32,33] The lattice thermal conductivity of PbTe is ∼2.2 W/(m·K) at room temperature and falls at higher temperature with a $1/T$ dependence.

Solid solutions of PbTe with PbSe and SnTe have been extensively investigated, and below room temperature they exhibit lower lattice thermal conductivities than PbTe itself. Yet, they do not possess higher ZT primarily because of the reduced power factor. At high temperatures (e.g., ∼600−800 K) the lattice thermal conductivities of $Pb_{1-x}Sn_xTe$[34−37] and $PbTe_{1-x}Se_x$[38−40] are approximately the same as that of PbTe, and therefore no ZT benefit is obtained.

Recently, modification of the density of states to create resonance states near the conduction and valence bands to increase the Seebeck coefficient have been proposed.[41−44] When Tl is substituted in PbTe a resonant state forms that is located in the valence band and can give p-type material.[39,45,46] This phenomenon was recently utilized effectively in the PbTe:Tl system where a large ZT (1.5 at 773 K) was attributed to an increase in the Seebeck coefficient compared to pure PbTe.[47] The increase in the density of states was supported experimentally with charge transport measurements and low temperature specific heat measurements. The thermal conductivity in this system, however, was not reduced compared to pristine PbTe. Extensive theoretical studies on the electronic structure of PbTe and the important role of defects in modulating the electronic structure and consequently the charge transport properties have been published.[41,43,48−52]

$AgPb_mSbTe_{2+m}$ (LAST-*m*)

The reaction of $AgSbTe_2$ with PbTe results in the $AgPb_mSbTe_{2+m}$ family of materials (LAST-*m*: lead antimony silver telluride). Early studies of this system reported it to be a solid solution between PbTe and $AgSbTe_2$ (both rock salt NaCl type structures) with p-type properties and an unusually low lattice thermal conductivity.[53,54] The average solid solution structure is shown in Figure 1. The belief that the system is a solid solution came from the fact that the LAST-*m* series does in fact follow Vegard's law (an often used "diagnostic" for solid solution behavior) when it comes to the dependence of the lattice constant with composition, Figure 2a.

At values of *m* up to ∼8, X-ray diffraction data clearly show a phase-separated system with two sets of diffraction

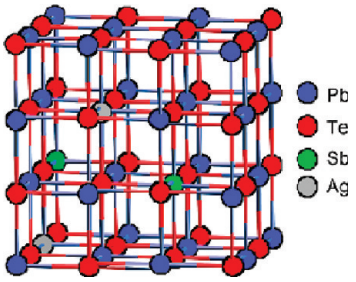

Figure 1. Average rock salt structure of the LAST-*m* system.

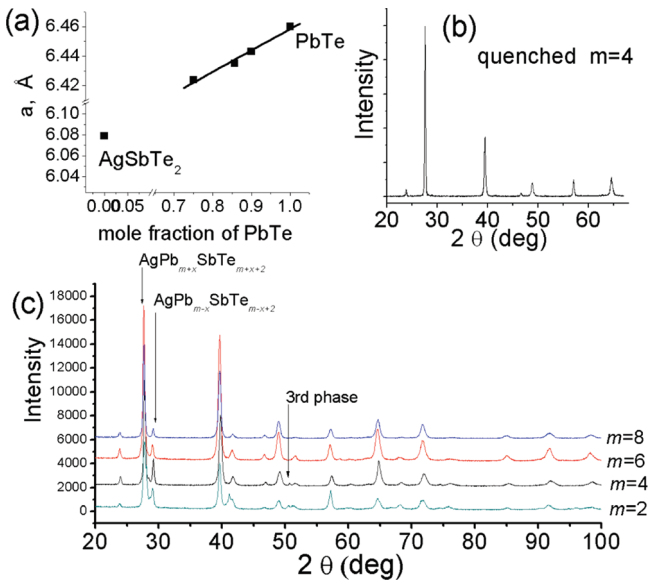

Figure 2. (a) Smooth variation of lattice constant in the $(AgSbTe_2)_{1-x}$-$(PbTe)_x$ system. (b) X-ray diffraction pattern of a quenched LAST-*m* sample consistent with single phase. (c) X-ray diffraction pattern of a slow cooled (or annealed) LAST-*m* sample showing microscopic phase segregation. The so-called "3rd phase" indicated in (c) is a minor impurity phase.

patterns being observed. Quenching these samples from the melt results in materials which appear to be single phase by standard X-ray diffraction, Figure 2b, but when these are annealed at ~400 °C phase separation occurs, Figure 2c. The phase separation gives rise to large regions of the two phases, and as a result the lattice thermal conductivity, though considerably reduced from that of PbTe, is higher than that of LAST-18.

When $m > 10$ the X-ray diffraction patterns indicate a "single phase"; however, transmission electron microscopy (TEM) shows extensive nanophase formation, and this is accompanied with a very low lattice thermal conductivity (see below). This seemingly single phase character is not retained in samples with low *m*-value that are cooled slowly below 500 °C, and massive phase segregation occurs in the low *m*-value members of the $AgPb_mSbTe_{m+2}$ ($m = 2, 4, 6, 8$) as observed by powder X-ray diffraction in Figure 2. It is clear there is a thermodynamic driving force for the phase segregation, and within the range $2 < m < 10$ the sample exhibits definitive biphasic composition. Since the phase segregation is observable with X-ray diffraction the system is not nanostructured but composed of large microscopic regions which do not provide any significant advantage in reducing lattice thermal conductivity (values vary around 1 W/(m·K)). This phase segregation behavior was not recorded in the published phase diagram; however, it is consistent with the recent calculation of the phase diagram of this system which also predicts phase segregation.[55,56]

We observed that n-type samples could be made by introducing Ag deficiency, which could then act as a way to control the carrier concentration. The LAST materials are thermally stable up to their melting point at >1200 K, and doping is generally controlled via nonstoichiometry on the Ag, Pb, or Sb fractions in the form of $Ag_{1-x}Pb_{m+y}Sb_{1+z}Te_{2+m}$. The LAST-*m* ($m \sim 18-22$) system showed high power factor and rather low lattice thermal conductivity giving a ZT ~ 1.7 at ~700 K.[57]

The LAST-*m* system proved to be a bulk material that spontaneously forms nanostructures during cooling from the melt. High figure of merit and nanoinclusions in the n-type $AgPb_mSbTe_{2+m}$ system were subsequently confirmed by follow up reports.[58,59] Because of the complex nature of the phase diagram, the thermoelectric properties of LAST are extremely sensitive to the synthesis conditions.[60] Even $AgSbTe_2$ itself, one of the end members of the pseudobinary mixture, is prone to phase segregation depending on composition and synthetic conditions.[61] The material separates into a two-phase mixture of a rock-salt phase, which is $Ag_{22}Sb_{28}Te_{50}$, and Ag_2Te. Ag_2Te formation results either from eutectic solidification (large lamellar structures) or by solid-state precipitation (fine-scale particles). There is a preferred crystallographic orientational relationship at the interface between the matrix and the low-temperature monoclinic Ag_2Te.

The lattice thermal conductivity of LAST-18 is estimated to be much lower than what is expected from a conventional solid solution compound. The power factor reported so far in the LAST system, though relatively high, is still lower than that of optimized PbTe itself, indicating that electron scattering in LAST is somewhat increased. Thus, the overall impact of the nanoinclusions in LAST-18 is a net enhancement of ZT compared to PbTe.

The nanoscale inclusions of minor phases in $AgPb_mSbTe_{2+m}$ exhibit coherent or semicoherent interfaces with the matrix. The inclusions form via nucleation and growth events during cooling. Cross-sectional transmission electron microscopy (TEM) shown in Figure 3 illustrates this relationship where coherence between the two regions is visible. This nanostructuring involves the endotaxial embedding of regions of one composition inside a matrix of another composition.[62] This seems to be a consequence of nucleation and growth of a second phase where coherent nanoscale inclusions form throughout the material, which is believed to result in scattering of acoustic phonons while causing only minimal scattering of charge carriers.

Characterization of the nanosized inclusions in LAST samples shows a strong tendency for crystallographic

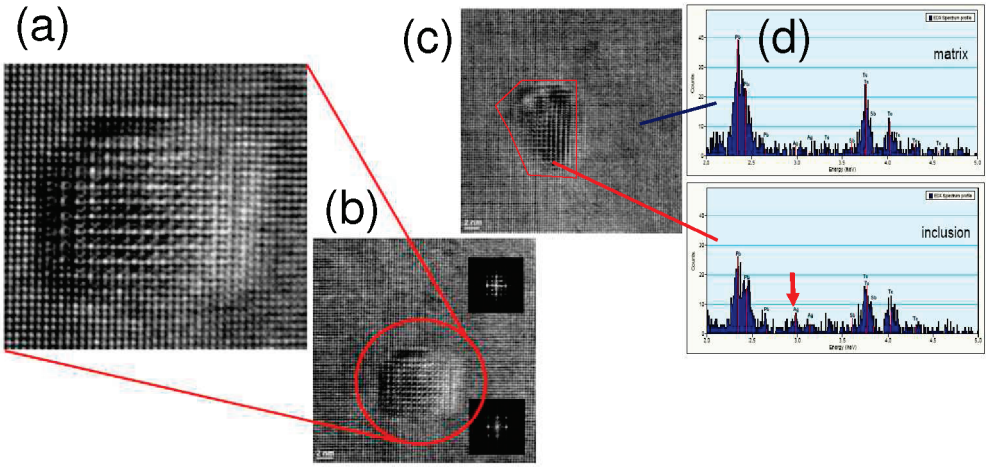

Figure 3. (a) High resolution image of an inclusion in $Ag_{0.53}Pb_{18}Sb_{1.2}Te_{20}$ along the [001] zone axis. (b) and (c) TEM micrograph of nanoscale inclusions in $Ag_{0.53}Pb_{18}Sb_{1.2}Te_{20}$. (d) EDS compositional profile of nanoinclusion shown in (c). Adapted with permission from ref 63.

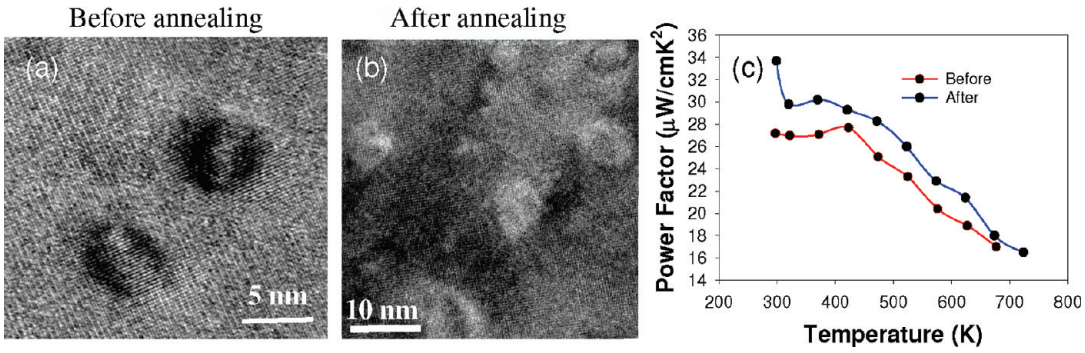

Figure 4. (a and b) High resolution transmission electron microscopy of a LAST-18 sample before and after annealing at 870 K, for a 3 month period in vacuum. (c) Power factor of the sample before and after annealing.

orientation along the {001} planes, with a high degree of lattice strain at the interface, consistent with a coherent interfacial boundary. The inclusions seem to be enriched in Ag relative to the matrix, Figure 3; however, considerably more characterization is required to fully understand what they are actually made of.[63]

Ab initio electronic structure calculations based on gradient corrected density-functional (DFT) theory performed on $AgPb_mSbTe_{2+m}$ materials indicated that the electronic structure near the gap depends sensitively on the microstructural arrangements of Ag−Sb atoms, suggesting that large ZT values may originate from the nature of these ordering arrangements. Such arrangements are of course a strong function of the cooling rates and annealing conditions of the samples, which is consistent with experimental observations.[64]

Are these nanostructures stable over long periods of time? The above arguments regarding nucleation and growth point to a thermodynamic and kinetic stability of the nanoinclusions in these materials. Therefore, long-term stability at high temperatures is expected, provided the temperature is not high enough to favor thermodynamic dissolution of the features. Such high temperatures for the LAST system are believed to be around 900 K and above. Below this, temperature stability of the features is expected. Even if the temperature exceeds 850 K and the features dissolve, they will reform as soon as the temperature drops below ~850 K. We tested the thermal stability of the LAST material by annealing samples at 870 K, for 3 months in vacuum (sealed silica tube). The samples were then examined to determine the presence of nanostructures and their thermoelectric properties. We found that the nanostructures were still present in the samples and the thermal conductivity and Seebeck remained unchanged, while the electrical conductivity improved by ~5−10%, Figure 4. This gave rise to a net increase in ZT with annealing time and has positive implications for the long-term operation of potential devices assembled from these materials. In an in situ high-temperature synchrotron radiation diffraction study we observed that the inclusions remain thermally stable to at least 800 K.[63]

Another approach to prepare LAST material is based on mechanical alloying and spark plasma sintering (SPS). Good thermoelectric performance was also obtained for LAST-*m* materials using this nanocomposite approach.[58] Polycrystalline $Ag_{0.8}Pb_{18+x}SbTe_{20}$ materials formed by mechanical alloying of elemental powders followed by densification through spark plasma sintering achieved a ZT of 1.5 at 673 K.[59] The average grain size of the nanocomposite was ~1 μm, with a compacted density of ~95% of the theoretical value. The observed ~20-nm-sized

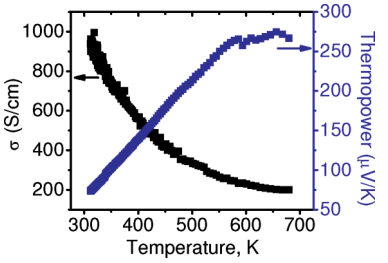

Figure 5. Temperature dependent electrical conductivity and thermoelectric power for the LASTT composition $Ag_{0.5}Pb_6Sn_2Sb_{0.2}Te_{10}$.

precipitates in the grains are believed to play an important role in lattice thermal conductivity reduction, similar to the melt grown materials.

$AgPb_mSn_nSbTe_{2+m+n}$ (LASTT)

When Pb atoms in the LAST system are gradually replaced with Sn atoms we obtain the $Ag(Pb_{1-y}Sn_y)_m$-$SbTe_{2+m}$ series (LASTT: lead, antimony, silver, tin tellurium). The introduction of Sn results in p-type materials.[65] ZT values for certain m and n values can reach 1.4 near 700 K. Presumably, the matrix in these nanocomposites is comprised of the $Pb_{1-x}Sn_xTe$ solid solution, and the nanoprecipitates are rich in Ag and Sb as was observed in LAST. In the LASTT materials the transport properties are not as easily tunable by varying the Ag or Sb concentrations as in the case of the Sn free n-type material. The transport behavior in LASTT is more easily tuned through the Pb/Sn ratio with the 9/9 composition giving the optimum values for power factor; however, other ratios such as 6:2 also give high power factor values. Electrical conductivity and Seebeck coefficient data from a typical optimized sample of LASTT are shown in Figure 5. The high performance of LASTT is linked to a very low lattice thermal conductivity (~0.5 W/(m·K)) which again is linked with the embedded coherent nanostructures found in these systems by HRTEM. The nanostructures are in the order of 3−20 nm and are generally coherent with the surrounding crystal matrix.

The derived κ_{latt}, for $AgPb_{12}Sn_4Sb_{0.4}Te_{20}$, $AgPb_{14}Sn_6$-$Sb_{0.4}Te_{24}$, and $AgPb_{10}Sn_{10}Sb_{0.67}Te_{22}$, in comparison with that of PbTe, is depicted in Figure 6. It can be readily seen that the lattice thermal conductivity of the LASTT system is only 40% that of PbTe at room temperature and ~50% at 620 K. This indicates significant changes in the lattice dynamics of this system at high temperatures deviating from the Debye-Peierls theory that predicts a scaling law, $\kappa_{latt} \sim 1/T$. Since there is no observed scaling in κ_{latt} with m and/or y in the $Ag(Pb_{1-y}Sn_y)_mSbTe_{2+m}$ nor with the introduction of point defects, the strong suppression of the intermediate frequency heat carrying phonons seems to be achieved via the existing nanostructuring.

$NaPb_mSbTe_{2+m}$ (SALT-*m*)

The sodium-substituted system $NaPb_mSbTe_{2+m}$ (SALT-*m*: sodium antimony lead telluride) is also a high

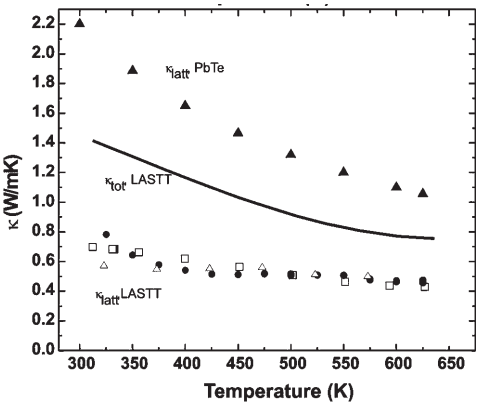

Figure 6. Lattice thermal conductivity for three compounds of the Ag-$(Pb_{1-y}Sn_y)_mSbTe_{2+m}$ series (open squares for $AgPb_{12}Sn_4Sb_{0.4}Te_{20}$, open triangles for $AgPb_{14}Sn_6Sb_{0.4}Te_{24}$, and bullets for $AgPb_{10}Sn_{10}Sb_{0.67}Te_{22}$) in comparison to that of PbTe. The solid line depicts the total κ of $Ag_{0.5}Pb_6Sn_2Sb_{0.2}Te_{10}$.

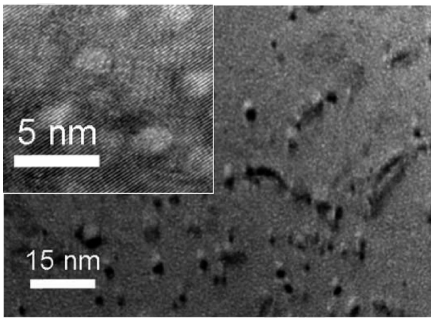

Figure 7. TEM image of SALT-18 materials clearly showing nanoscale precipitates. Inset: high resolution magnified image of a SALT-18 sample.

performance system (ZT ~ 1.6 at 675 K for $m \sim 20$)[66] but has p-type behavior. Again, the high ZT comes from the very low thermal conductivity of the material which is as low as 0.85 W/(m·K), of which ~0.5 W/(m·K) corresponds to the lattice contribution. HRTEM images show a broad-based nanosegregated system with features similar to those exhibited by the LAST samples, see Figure 7. In similar fashion to LAST, the SALT system naturally creates Na−Sb-rich clusters in the lattice. The distribution of Na^+ and Sb^{3+} ions in the Pb^{2+} sublattice cannot be random as would be demanded by a solid solution, because Coulombic forces alone tend to drive the system into clustering at the nanoscale thereby lowering the overall energy.[67] High power factors can be obtained by optimizing the Na/Sb ratio, Figure 8. As a result, the ZT of $Na_{0.95}Pb_{20}SbTe_{22}$ climbs sharply with temperature and reaches 1 near 475 K and ~1.7 at 650 K. This is one of the widest temperature ranges in which a single material exhibits ZT above 1. The Bi analogue $NaPb_{18}BiTe_{20}$ is also a promising material reaching a ZT ~ 1.3 at 670 K. Its lattice thermal conductivity is slightly higher (0.7 W/(m·K)) than that of the $NaPb_{18}SbTe_{20}$.[68]

Corresponding studies of $NaPb_mSn_nSbTe_{m+n+2}$ materials (SALTT) indicated that their TE performance did not exceed those of the SALT-*m* systems.[68] This is mainly because of the inferior power factor properties. These materials, however, also proved to be nanostructured and

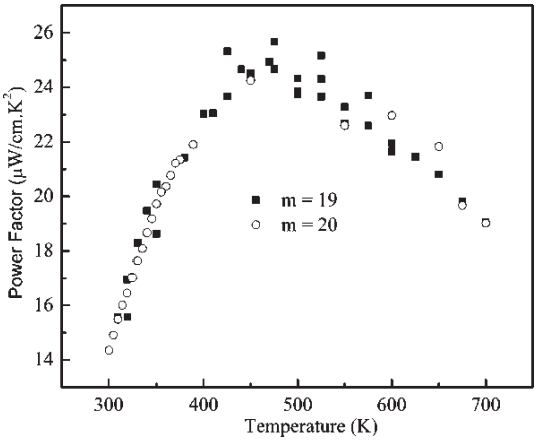

Figure 8. Power factors for SALT-19 and SALT-20 samples.

exhibit very low thermal conductivities. The $NaPb_{18-x}Sn_xMTe_{20}$ (M = Sb, Bi) series exhibits increasing total thermal conductivity with Sn fraction with room temperature values between 1.37 W/(m·K) for $x = 3$ and 3.9 W/(m·K) for $x = 16$. The lowest lattice thermal conductivity, ~0.4 W/(m·K), was observed for the composition $NaPb_2Sn_{16}BiTe_{20}$ at 650 K. High-resolution transmission electron microscopy on several members of the $NaPb_{18-x}Sn_xMTe_{20}$ series reveals that they are inhomogeneous on the nanoscale with widely dispersed nanocrystals embedded in a $Pb_{1-y}Sn_yTe$ matrix. Also observed are lamellar features in these materials associated with compositional fluctuations and significant strain at the nanocrystal/matrix interface, Figure 9a.

Image processing for strain field analysis was used to investigate the variation in lattice parameters, and thus the elastic strain, at and around these layers. Figure 9b shows the power spectrum (from FFT) of the image in Figure 9a with $\mathbf{g_1} = 002$ and $\mathbf{g_2} = 220$ chosen as the Fourier vectors. The strain map profiles along the 001 direction (ε_{yy}) and the shear direction (ε_{xy}) are shown in Figure 9c−f. There is about 6% difference between lamella A and B, inferred from the power spectrum, indicating different lattice parameters. It is possible that the lamellar features may be due to local ordering between PbTe and SnTe phases, though definitive proof would require additional EDS studies, which are underway.

Notwithstanding the detailed chemical makeup of the constituents, it is obvious that complex nanostructures and concomitant interface-induced matrix perturbations are ubiquitous in these systems. We have proposed that such nanostructure and interface-induced matrix elastic perturbations play a decisive role in mediating the phonon propagation pathway and thus contribute to enhanced phonon scattering resulting in reduced thermal conductivity in these systems.[68,69]

KPb_mSbTe_{2+m} (PLAT-*m*)

More recently we explored the K-based analogues of the p-type $Na_{1-x}Pb_mSb_yTe_{m+2}$ materials which have the tendency to be n-type. The $K_{1-x}Pb_{m+\delta}Sb_{1+\gamma}Te_{m+2}$

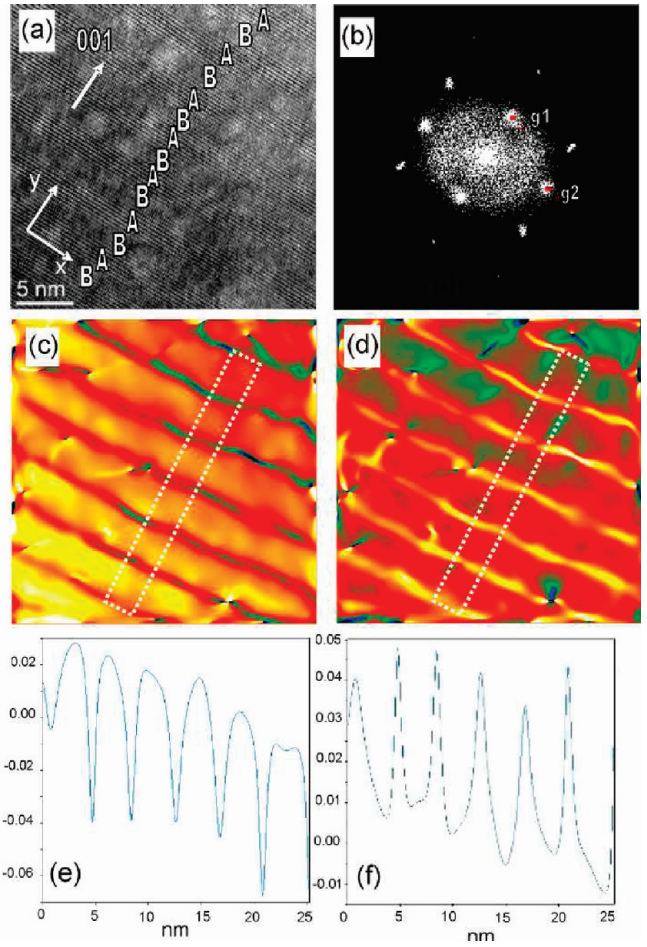

Figure 9. (a) Different precipitate from $NaPb_{13}Sn_5BiTe_{20}$ with different contrast lamella structure labeled as ABAB... (b−f) are strain mapping for this precipitate; (b) power spectrum image in (a) with $\mathbf{g_1} = 002$ and $\mathbf{g_2} = 220$. (c and d) [e and f] Strain map profile along the 001 direction (ε_{yy}) and the shear direction (ε_{xy}), respectively.

materials system (PLAT-*m* for potassium−lead−antimony−tellurium) exhibits the same low lattice thermal conductivity as the SALT-*m* system and thus offers an additional proof of the strong influence of the alkali metal on the reduction of the lattice thermal conductivity of PbTe-based materials. As a result, a maximum ZT of ~1.60 at 750 K was achieved for the composition $K_{0.95}Pb_{20}Sb_{1.2}Te_{22}$. Combined HRTEM and thermal conductivity data on $K_{1-x}Pb_{m+\delta}Sb_{1+\gamma}Te_{m+2}$ clearly show the nanostructured nature of the PLAT-*m* system, Figure 10. The primary reason for this nanostructuring is the strong tendency of alkali metal and Sb to promote the formation of stable nanocrystals that are coherently embedded in the PbTe-rich matrix and serve as additional phonons scattering centers with less impact on the electron flow. The stability of the thermoelectric properties of $K_{1-x}Pb_{m+\delta}Sb_{1+\gamma}Te_{m+2}$ and $Na_{1-x}Pb_mSbTe_{m+2}$ materials upon small variation of the composition is a strong indication of the potential for successful scale-up synthesis (see full article elsewhere in this issue).[70]

PbTe−PbS

The discovery of nanodots in the LAST-*m* and SALT-*m* systems, coupled with the results observed in superlattice

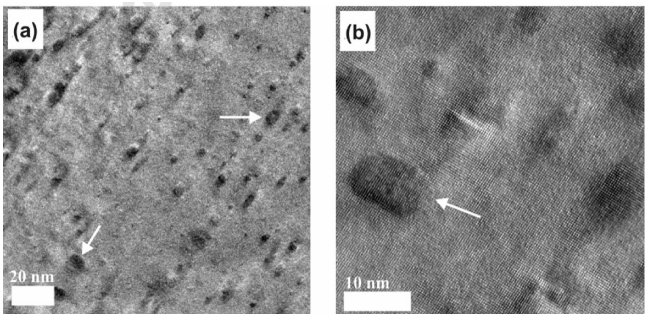

Figure 10. HRTEM images of $K_{1-x}Pb_{20+\delta}Sb_{1+\gamma}Te_{22}$ ($m = 20$) samples. (a) Low magnification TEM image of $K_{0.95}Pb_{20}SbTe_{22}$ showing nanometer size crystalline K/Sb-rich particles inside PbTe-rich matrix. (b) The corresponding high magnification image showed coherently particles/matrix boundaries.

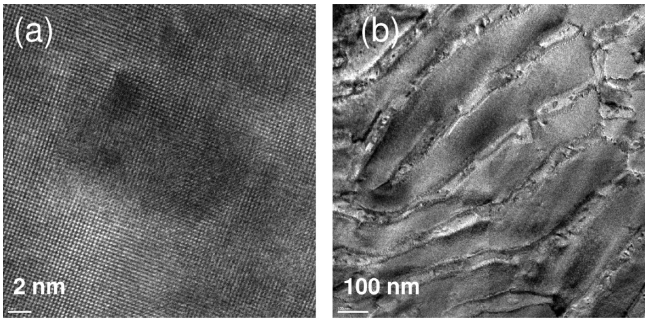

Figure 11. Transmission electron microscope images of (a) PbTe-PbS-(8%) showing a PbS precipitate and (b) PbTe-PbS(30%) showing compositional fluctuations formed in the sample through phase segregation and spinodal decomposition.

and endotaxially embedded nanocrystalline thin films, points to a new paradigm in thermoelectric materials exploration. This paradigm involves nanostructuring PbTe and other promising materials with a variety of inclusions to achieve record low lattice thermal conductivity for the particular system. Solid state phenomena such as spinodal decomposition and nucleation and growth constitute nearly ideal mechanisms for the formation of phonon-scattering inclusions because by its nature the precipitate phase undergoes a series of coarsening steps with coherent or semicoherent interfaces during the early stages. Consequently, their composition and structure, as well as size and distribution, can be controlled through judicious selection of cooling rate and post synthesis heat treatment. Spinodal decomposition is known to occur in the PbTe−PbS system, and we have shown that precipitates of PbS are embedded in the PbTe matrix. We found that the PbTe−PbS system actually exhibits three scales of inhomogeneity, Figure 11. The system $(PbTe)_{1-x}(PbS)_x$ does not form a solid solution, but rather phase separates into PbTe-rich and PbS-rich regions to produce coherent nanoscale heterogeneities.[71,72] For $x > \sim 0.03$, the materials are ordered on three submicrometer length scales. The coherent nanoinclusions in $(Pb_{0.95}Sn_{0.05}Te)_{1-x}(PbS)_x$ do not result in excessive electron scattering, and high electron mobilities of >100 cm^2/(V·s) are observed at 700 K. At $x \sim 0.08$ the material achieves a very low room temperature

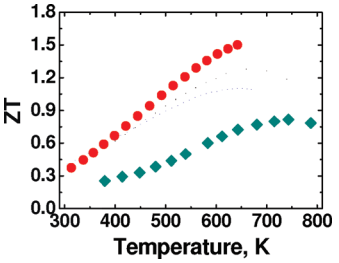

Figure 12. Measured ZT for a PbTe-PbS(8%) nanostructured material (red points) doped with PbI_2 showing vast improvement over a corresponding sample of optimized pure PbTe (also doped with doped with PbI_2).

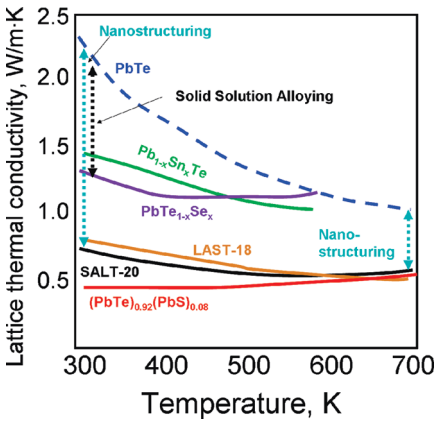

Figure 13. Lattice thermal conductivity as a function of temperature for various PbTe-based alloys and nanostructured samples.

lattice thermal conductivity (~30% that of PbTe), and a ZT ~ 1.5 at 650 K is possible, Figure 12.[71]

In addition to nanostructuring, the systems typically have other coexisting defects, including solid solution behavior. An important question to ponder then is how much of the observed reduction in thermal conductivity in these systems is explicitly from the nanodots and how much from the point defects. Figure 13 shows a comparison of lattice thermal conductivities for five PbTe-based materials systems plus pure PbTe. It is clear that while solid-solution point defect scattering alone is effective in lowering the κ_{latt} of PbTe by ~30−40% the nanostructuring contributes additional significant phonon scattering mechanisms for an overall ~70−75% reduction.

Nanostructured PbTe by Liquid Encapsulation

In general, bulk crystals embedded with nanocrystals in them represent a fascinating set of nanostructured materials whose scope actually extends beyond the field of thermoelectrics especially when the properties of guest/matrix are chosen for specific functions. We have proposed a convenient method on how to introduce a variety of materials in PbTe and in related semiconductors called "matrix encapsulation".[73] As we have described earlier, to achieve nanoscale matrix encapsulation of a minority phase A inside a majority phase B, the former must have very low or no solubility in the solid state but complete solubility in the liquid state. The major phase B should have an equal or higher melting point than

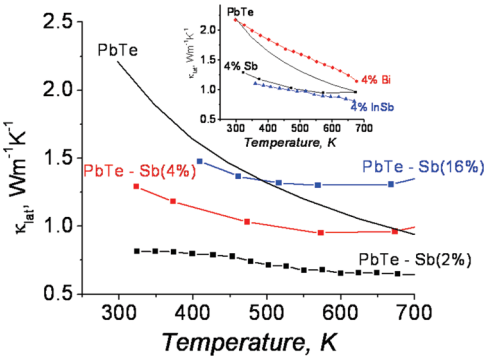

Figure 14. Comparison of lattice thermal conductivities of PbTe nanostructured with varying amounts of inclusion of Sb, as well as Bi and InSb (inset). The maximum reduction in thermal conductivity is observed at 1.5−2% Sb. For similar fractions with Bi inclusions (or Pb) no reduction is observed.

the minor phase (guest or inclusion) so that on rapid cooling it will be first to solidify thereby precipitating and simultaneously encapsulating nanocrystals of phase A.[73] These conditions are akin to what is known in conventional solution chemistry as arrested precipitation.[74−77] This is a general method to prepare bulk nanostructured materials of thermoelectric interest provided the matrix is chosen to be an already promising thermoelectric. The minor phase could be a nonreactive material capable of altering the phonon scattering processes of the medium.

Strong reductions in lattice thermal conductivity have been observed in PbTe samples containing $<3\%$ nanoparticles of Sb, Figure 14.[73] In contrast, similar fractions of nanoparticles of Bi or Pb (two elements that have the similar atomic mass as the Pb ions in the rock salt lattice) were found to have no such effect.[73,78] Mass contrast between nanoparticles and matrix is apparently important when considering which nanostructured materials to investigate to achieve low thermal conductivity. The presence of Pb and Bi nanodots, for example, does not result in a significant reduction of the thermal conductivity even though the nanoparticle size distribution of these phases is very similar to that of Sb (for similar concentrations). Of course, the mass of Pb and Bi atoms in the nanoparticles is nearly identical to the mass of the Pb atoms in the PbTe matrix, and the phonons may not be able to sense the difference (acoustic mismatch), Figure 14.

These results underscore the important role properly chosen nanoparticles play in enhancing phonon scattering in PbTe. We learned that there is an optimum concentration of Sb nanoparticles (e.g., 1.5−2%) and not a maximum concentration that maximizes the phonon scattering. Thus, we have to conclude that the observed reduction in lattice thermal conductivity is not simply due to a disruption of the PbTe matrix caused by introducing more and more of a second phase into it. In this case we would expect either the opposite trend with nanoinclusion concentration (i.e., higher nanoparticle concentration causing greater reduction in the thermal conductivity) or a trend consistent with the "law of mixtures" (i.e., the thermal conductivity would be an average of the two individual components). Presumably the optimum concentration yields an optimum nanoparticle size distribution (~2−20 nm) with an overall very high interface area between the Sb and the PbTe for maximum phonon scattering to occur.[79] As the concentration of Sb increases, the average particle size increases (e.g., 4−50 nm) which probably results in a decrease in the interface area and concomitant loss of the full effect of phonon scattering. Presumably then, if there was a way to keep the nanoparticle size distribution small (e.g., 2−10 nm) and further increase the concentration of the nanoparticles, we may expect even further reductions in the lattice thermal conductivity.

The current insight that "particles in a matrix" nanostructuring can lead to dramatic reductions in thermal conductivity (well below the alloy limit) is supported by several other studies that do not involve PbTe. One example is the careful work on the InGaAs: ErAs thin films. The InGaAs:ErAs system contains ErAs nanoparticles endotaxially embedded in a InGaAs matrix. The size distribution of ErAs nanoparticles in the matrix of InGaAs is typically 2−4 nm in diameter.[80] Thermal conductivity measurements show a reduction by as much as a factor of 3 compared to the bulk alloy. Detailed calculation of the phonon transport in ErAs:InGaAs for various nanoparticle sizes and distributions has shown that the significant reduction in lattice thermal conductivity is due to the scattering of mid- and long-wavelength phonons by the nanoparticles. These phonons are not effectively scattered by the point defects in a bulk alloy, which are more effective at scattering short-wavelength phonons.

Recently, PbTe co-nanostructured with both Pb and Sb precipitates has shown novel temperature dependent behavior of the electron mobility, and enhancements at high temperature result in increased ZT to 1.4 at 673 K.[81] Co-nanostructuring may also present a method for increasing the power factor of thermoelectric materials as both an increased power factor and reduced thermal conductivity were observed in one material. For a given carrier concentration we observe an increased electrical conductivity at high temperatures which is responsible for increasing the power factor, Figure 15a. This increased electrical conductivity is a result of higher than expected mobility at high temperatures. The temperature dependence of the mobility in PbTe typically follows a power law ($\mu \sim T^{-2.5}$); however, in PbTe nanostructured with Pb and Sb the temperature dependence can be tuned by the Pb/Sb ratio. This leads to larger than expected mobilities at high temperature because the mobility falls more slowly than in PbTe itself. This behavior is not observed in PbTe with Pb or Sb precipitates alone. It would appear that a synergy between the two types of precipitates may be the cause of this unique behavior. Additionally, for the PbTe-Pb(0.5%)-Sb(2%) composition a substantial decrease in the lattice thermal conductivity was also observed leading to a ZT ~ 1.5 at 700 K, Figure 15b. The exact mechanism and further understanding in this

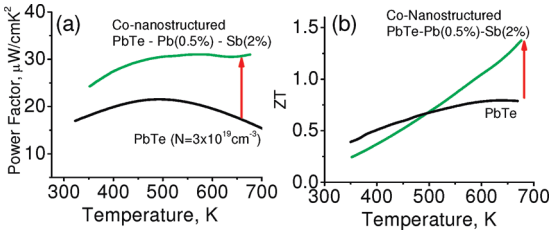

Figure 15. PbTe conanostructured with Pb and Sb: (a) Power factor for showing a clear enhancement (~71%) over PbTe of the same carrier concentration. (b) ZT comparison with optimized PbTe.

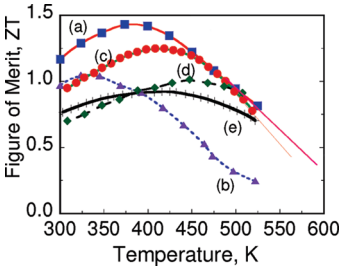

Figure 16. Figure of merit ZT as a function of temperature for bulk $Bi_{2-x}Sb_xTe_3$ and $Bi_2Te_{3-x}Se_x$ materials prepared by (a) ball milling and hot pressing (p-type), (b) zone melting (p-type), (c) melt spinning and SPS (p-type), and (d) hydrothermal synthesis (n-type) and (e) conventional $Bi_{2-x}Sb_xTe_3$.

composite may shed light on mechanisms that could be applied generally to many other thermoelectrics.

In related work we prepared thermoelectric materials based on the eutectic phase relationship between PbTe and Ge.[82] When quenched, these eutectic mixtures exhibit considerably stronger mechanical strength and reduced brittleness compared to PbTe itself, while at the same time they possess lower lattice thermal conductivity. Thermal conductivity measurements show values lower than expected based on the law of mixtures and multiphase composites. The thermoelectric performance in these composites can be tuned through the use of hypereutectic compositions and alloying of Ge with Si and through carrier doping. ZT values approaching 1.3 at 778 K have been obtained in samples of PbTe-$Ge_{0.8}Si_{0.2}$-(5%), which represent a 62% improvement over that of PbTe.[82] In general, the mechanical properties of thermoelectric materials such as those which are PbTe based have not received adequate attention until recently.[83−92]

Nanocomposite Polycrystalline Materials

The nanostructuring modalities described above are "nanoparticles in a matrix". There are other approaches to achieve nanostructuring and include the formation of nanosized (grain size ~5 nm−10 μm) polycrystalline samples formed by grinding and milling or wet chemistry processing, followed by hot pressing or spark plasma sintering of fine powders. Nanoparticles of the thermoelectric material can also be prepared separately with "wet chemical methods" which are then compacted into dense samples by hot pressing or spark plasma sintering. Instead of the nanoparticles in a matrix model described above, this approach creates extensive interfacing between the compacted nanoparticles which can lower the thermal conductivity. The resulting sample can exhibit certain benefits over techniques that create very large-grain or single crystal material, such as reduced thermal conductivity (due to phonon scattering at grain boundaries), increased power factor (due to electron filtering at grain boundaries), better mechanical properties, and improved isotropy. Compacting nanocrystalline samples can be a relatively low-cost method to provide the large volume of material necessary for more widespread adoption of thermoelectrics.[93] However, a major challenge with this approach is obtaining complete removal of the oxide layers and any binder or organics used in the grinding, milling, or wet chemistry processes, as well as obtaining highly dense samples during compaction. If this is not successful, the carrier mobility will be low and the thermoelectric properties poor.[6] This technique has been applied to several different classes of materials including PbTe[94−96] Bi_2Te_3,[8,93] and skutterudites.[97−100]

Promising results have been reported with n-type nano/polycrystalline Bi_2Te_3 material resulting in a higher ZT ~ 1.25 at 420 K compared to bulk Bi_2Te_3, Figure 16.[8] This material was prepared via hot pressing of nanometer sized n-type Bi_2Te_3 and micrometer sized powders mixed together. The improvement in ZT was attributed to a slight increase in electrical conductivity and a reduction (~25%) in thermal conductivity. Additionally, Poudel et al.[93] obtained ZT of 1.2 at room temperature and 1.4 at 373 K from a ball-milled and hot-pressed p-type BiSbTe alloy, Figure 16. These values are about 20 and 40% higher, respectively, than the comparable state-of-the-art ingot BiSbTe alloy results they reported, with even greater improvement observed at higher temperatures. Surprisingly, the observed electrical conductivity for the nanostructured material was also higher than the ingot material, similar to the nanograined n-type material previously reported.[8] The Seebeck coefficient was higher or lower depending on the temperature, yielding a slightly enhanced power factor for the nanostructured material. The improvement in ZT was attributed to a strongly reduced thermal conductivity and slightly increased power factor for the nanostructured material compared to the ingot, particularly at elevated temperatures. Using this nanostructured p-type material and a commercial n-type leg, a ~20 °C greater cooling capacity was reported compared to using commercial material for both the p- and n-legs. The thermal stability of these systems can be an issue because at high temperatures grain growth and grain fusion will result in permanent loss of the nanocrystallinity and in reversion to the conventional BiSbTe alloy with concomitant loss of the high ZT.[101] Therefore, it is possible these systems may be limited in temperatures below those that promote grain growth.

Recently, PbTe nanocomposites prepared by densifying ~100 nm PbTe nanocrystals (synthesized via a solution-phase technique) within a dense Ag-doped PbTe matrix were reported.[102] These samples had a unique temperature

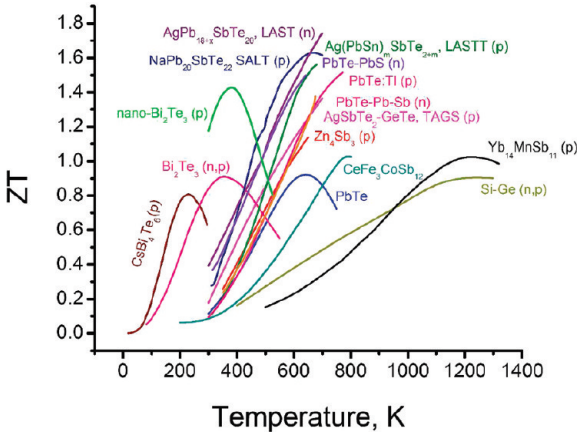

Figure 17. Current state of the art in bulk thermoelectric materials.

dependence of mobility which was attributed to an additional scattering mechanism in combination with the classical phonon-carrier scattering dominant in conventional PbTe. The additional scattering mechanism was proposed to arise from the metal oxide epilayer around the nanoparticle which may result in energy barriers that impede the conduction of carriers between grains. This conduction can then be effectively described as dominated by grain-boundary potential barrier scattering, coexisting with phonon scattering.[102] These nanocomposites showed an enhanced thermoelectric performance as compared to bulk PbTe suggesting that interfacial energy barrier carrier scattering is an effective method of ZT enhancement in bulk nanocomposites.

Nanocomposite boron-doped Si/Ge materials formed by ball milling and hot pressing were reported[6] to exhibit increased Seebeck coefficients and only slightly reduced electrical conductivities compared to bulk SiGe alloys, resulting in a higher power factor for the nanocomposite material over the temperature range of 300−1000 K. The increased power factor for the nanocomposite is similar to what was observed for the BiSbTe alloy above and as predicted based on electron filtering effects at the grain boundaries. In addition, the thermal conductivity of the n-type Si/Ge alloy ($Si_{80}Ge_{20}P_2$) nanocomposite was significantly reduced over the entire temperature range, resulting in a peak ZT of ~1.3 at 1200 K compared to a value of ~0.9 for the bulk SiGe alloy.[103,104]

Conclusions and Insights

The new idea in thermoelectric materials in the past 10 years or so is the concept of nanostructuring. In nanostructured systems enhanced thermoelectric performance can be produced from a strong decrease in the lattice thermal conductivity.[105−108] The nanoinclusions are believed to effectively scatter phonons that otherwise would have relatively long mean free paths. The ZT values of the current state of the art thermoelectric materials are shown in Figure 17, although this "landscape" is now rapidly evolving because of continued advances in the field. At this point in time all top performing materials are nanostructured.

Numerous results suggest that a wide size distribution of nanoparticles can effectively scatter different phonon modes and reduce thermal conductivity. These discoveries have changed the way we think about thermoelectrics and opened new opportunities for designing "built in" nanostructuring in semiconductors.

Nanostructuring of thermoelectric materials for enhanced ZT is thus gaining momentum as the new broadly applicable paradigm to many bulk materials.[109,6] Recent reports on skutterudites[100] and half-Heusler alloys containing nanoinclusions confirm real enhancements in ZT via a thermal conductivity reduction. Despite this progress, the factors that control the nanostructural evolution in solids and the detailed mechanisms by which the nanostructural features enhance the thermoelectric performance need to be better understood.

How low can the thermal conductivity of PbTe-based systems go? The lowest experimentally estimated value is ~0.5 W/(m·K) from 300 to 700 K (e.g., PbTe-PbS). The 0.33 W/(m·K) claimed for the molecular beam epitaxy (MBE) grown thin film PbTe−PbSe superlattice systems is now in doubt.[4] To assess the lower practical thermal conductivity limits of these systems we grew nanoparticles of LAST-*m* and PbTe using inverse micelle "wet" chemistry methods with narrow size dispersity and an average size of 9−12 nm. After complete characterization these nanoparticles were processed into pellets by cold pressing, and their thermal conductivity was measured. The capping ligands used to stabilize these were either left on the nanoparticles or removed with only a small effect on the measurement results. Even though the pressed pellets did not achieve theoretical density, the measured total room temperature thermal conductivity values were ~0.40−0.50 W/(m·K). Since these pellets were essentially electrically insulating, ~0.40−0.50 W/(m·K) represents the lattice thermal conductivity and thus the lowest possible achievable value for any PbTe-based material. It is difficult to imagine how it can be reduced much lower. Therefore, based on the above, future large ZT enhancements, at least for PbTe, will not come from further thermal conductivity reductions but from big jumps in the power factor from current levels. This is the main challenge going forward.

Therefore, mechanisms such as the exploitation of resonance states in semiconductors[39,45] hold promise and can be better guided by theoretical prediction.[41,44] One example is the PbTe:Tl system where resonance states can increase the Seebeck coefficient and the overall power factor at high temperature,[47] and if these properties could be coupled with the reductions in thermal conductivity mentioned above, much higher ZTs would result. Moreover, large increases in carrier mobility and power factor brought about by complex nanostructures, as in the conanostructured PbTe−Pb−Sb system,[81] are also promising and may also be applied to numerous systems if additional theoretical understanding of this phenomenon can be formulated.

Theoretical calculations on thermoelectric nanocomposite materials consisting of granular regions suggest

that by changing the physical characteristics of the nanocrystal, such as potential barrier height, width, and the distance between them, it is possible to increase the mean energy per carrier to obtain an enhanced power factor for improved thermoelectric performance. The model is promising and can be generic because it can be applied to other nanocomposites by incorporating the appropriate electronic structure parameters.[110]

Additionally, extensive work has also focused on understanding the mechanical properties of PbTe-based systems which is useful information when considering device fabrication.[111−113]

It is evident that the field of thermoelectrics now needs new bold theoretical guidance on how the power factor can be enhanced by 2−4-fold in the existing leading materials, especially enhancements that derive from the thermopower. Theorists in the field are urged to take risks.

Acknowledgment. The author is grateful to the Office of Naval Research for financial support (Grants N00014-02-1-0867, N00014-03-1-0789, N00014-06-1-0130, N00014-08-1-613). I thank Professors S.D. Mahanti, T.P. Hogan, C. Uher, V. Dravid, E. Case, A.J. Freeman, and C. Wolverton for plentiful stimulating discussions and fruitful collaborations. Of course most of all, I am grateful to the numerous dedicated graduate students and postdoctoral fellows who have contributed to our thermoelectric research effort. Their names appear in the various publications cited in this article.

References

(1) Wood, C. *Energy Convers. Manage*. **1984**, *24*, 331–343.
(2) Venkatasubramanian, R.; Siivola, E.; Colpitts, T.; O'quinn, B. *Nature* **2001**, *413*(6856), 597–602.
(3) Harman, T. C.; Taylor, P. J.; Walsh, M. P.; Laforge, B. E. *Science* **2002**, *297*(5590), 2229–2232.
(4) Koh, Y. K.; Vineis, C. J.; Calawa, S. D.; Walsh, M. P.; Cahill, D. G. Appl. Phys. Lett. **2009**, *94*, (15).
(5) Chen, G.; Dresselhaus, M. S.; Dresselhaus, G.; Fleurial, J. P.; Caillat, T. *Int. Mater. Rev*. **2003**, *48*(1), 45–66.
(6) Dresselhaus, M. S.; Chen, G.; Tang, M. Y.; Yang, R.; Lee, H.; Wang, D.; Ren, Z.; Fleurial, J.-P.; Gogna, P. *Adv. Mater*. **2007**, *19*, 1043.
(7) Rowe, D. M. *CRC Handbook Of Thermoelectrics*; CRC Press: Boca Raton, 1995
(8) Rowe, D. M. *Thermoelectrics Handbook: Macro To Nano*; CRC/Taylor & Francis: Boca Raton, 2006; and references therein.
(9) Slack, G. A. New Materials And Performance Limits For Thermoelectric Cooling. In *CRC Handbook Of Thermoelectrics*; Rowe, D. M., Ed.; CRC Press: Boca Raton, 1995; pp 407−440.
(10) Kim, S. J.; Hu, S. Q.; Uher, C.; Hogan, T.; Huang, B. Q.; Corbett, J. D.; Kanatzidis, M. G. *J. Solid State Chem*. **2000**, *153*(2), 321–329.
(11) Schujman, S. B.; Nolas, G. S.; Young, R. A.; Lind, C.; Wilkinson, A. P.; Slack, G. A.; Patschke, R.; Kanatzidis, M. G.; Ulutagay, M.; Hwu, S. J. *J. Appl. Phys*. **2000**, *87*(3), 1529–1533.
(12) Beekman, M.; Nolas, G. S. *Phys. B: Condens. Matter* **2006**, *383*(1), 111–114.
(13) Beekman, M.; Nolas, G. S. *J. Mater. Chem*. **2008**, *18*(8), 842–851.
(14) Bentien, A.; Pacheco, V.; Paschen, S.; Grin, Y.; Steglich, F. *Phys. Rev. B* **2005**, *71*(16), 165206.
(15) Donga, J.; Sankey, O. F.; Ramachandran, G. K.; Mcmillan, P. F. *J. Appl. Phys*. **2000**, *87*, 7726–7734.
(16) Kim, J.-H.; Okamoto, N. L.; Kishida, K.; Tanaka, K.; Inui, H. *Acta Mater*. **2006**, *54*, 2057–2062.
(17) Nolas, G. S. Structure, Thermal Conductivity, And Thermoelectric Properties Of Clathrate Compounds. In *Thermoelectrics Handbook: Macro- To Nano-Structured Materials*; Rowe, D. M., Ed.; CRC Press: Boca Raton, 2006; pp 34-1−13.
(18) Nolas, G. S.; Beekman, M.; Gryko, J.; Lamberton, G. A.Jr.; Tritt, T. M.; McMillan, P. F. *Appl. Phys. Lett*. **2003**, *82*(6), 910–912.
(19) Sales, B. C.; Chakoumakos, B. C.; Mandrus, D.; Sharp, J. W. *J. Solid State Chem*. **1999**, *146*(2), 528–532.
(20) Saramat, A.; Svensson, G.; Palmqvist, A. E. C.; Stiewe, C.; Mueller, E.; Platzek, D.; Williams, S. G. K.; Rowe, D. M.; Bryan, J. D.; Stucky, G. D. *J. Appl. Phys*. **2006**, *99*, 023708-5.
(21) Tritt, T. M.; Boettner, H.; Chen, L. *MRS Bull*. **2008**, *33*(4), 366–368.
(22) Disalvo, F. J. *Science* **1999**, *285*, 703–706.
(23) Kanatzidis, M. G. The Role Of Solid State Chemistry In The Discovery Of New Thermoelectric Materials. In *Semiconductors And Semimetals*; Tritt, T. M., Ed.; Academic Press: San Diego, 2000; Vol. *69*, pp 51−100.
(24) Sales, B. C. *Science* **2002**, *295*(5558), 1248–1249.
(25) Snyder, G. J.; Toberer, E. S. *Nat. Mater*. **2008**, *7*(2), 105–114.
(26) Nolas, G. S.; Poon, J.; Kanatzidis, M. *Mater. Res. Soc. Bull*. **2006**, *31*(3), 199–205.
(27) Chung, D. Y.; Iordanidis, L.; Choi, K. S.; Kanatzidis, M. G. *Bull. Kor. Chem. Soc*. **1998**, *19*(12), 1283–1293.
(28) Mrotzek, A.; Kanatzidis, M. G. *Acc. Chem. Res*. **2003**, *36*(2), 111–119.
(29) Sootsman, J. R.; Chung, D. Y.; Kanatzidis, M. G. Angew. Chem., Int. Ed. **2009**, in press.
(30) Medlin, D. L.; Snyder, G. J. *Curr. Opin. Colloid Interface Sci*. **2009**, *14*(4), 226–235.
(31) Minnich, A. J.; Dresselhaus, M. S.; Ren, Z. F.; Chen, G. *Energy Environ. Sci*. **2009**, *2*(5), 466–479.
(32) Dughaish, Z. H. *Phys. B: Condens. Matter* **2002**, *322*(1−2), 205–223.
(33) Yu, I.; Ravich, B. A. E.; Smirnov, I. A. *Semiconducting Lead Chalcogenides*; Plenum Press: New York, 1970; Vol. *5*.
(34) Hewes, C. R.; Adler, M. S.; Senturia, S. D. *J. Appl. Phys*. **1973**, *44*(3), 1327–1332.
(35) Wagner, J. W.; Woolley, J. C. *Mater. Res. Bull*. **1967**, *2*(11), 1055–&.
(36) Strauss, A. J. *Trans. Metall. Soc. AIME* **1968**, *242*(3), 354–&.
(37) Orihashi, M.; Noda, Y.; Chen, L.; Hirai, T. *J. Jpn. Inst. Met*. **1999**, *63*(11), 1423–1428.
(38) Kudman, I. *J. Mater. Sci*. **1972**, *7*(9), 1027–1029.
(39) Kaidanov, V. I.; Nemov, S. A.; Ravich, Y. I. *Soviet Physics Semiconductors-USSR* **1992**, *26*(2), 113–125.
(40) Alekseeva, G. T.; Gurieva, E. A.; Konstantinov, P. P.; Prokofeva, L. V.; Fedorov, M. I. *Semiconductors* **1996**, *30*(12), 1125–1127.
(41) Hoang, K.; Mahanti, S. D. *Phys. Rev. B: Condens. Matter Mater. Phys*. **2008**, *78*(8), 085111/1–085111/8.
(42) Bilc, D.; Mahanti, S. D.; Quarez, E.; Hsu, K. F.; Pcionek, R.; Kanatzidis, M. G. Phys. Rev. Lett. **2004**, *93*, (14).
(43) Ahmad, S.; Hoang, K.; Mahanti, S. D. *Phys. Rev. Lett*. **2006**, *96*(16), 056403.
(44) Ahmad, S.; Mahanti, S. D.; Hoang, K.; Kanatzidis, M. G. *Phys. Rev. B: Condens. Matter Mater. Phys*. **2006**, *74*(15), 155205/1–155205/13.
(45) Kaidanov, V. I.; Nemov, S. A. *Soviet Physics Semiconductors-USSR* **1981**, *15*(3), 306–311.
(46) Kaidanov, V. I.; Nemov, S. A.; Ravich, Y. I.; Zaitsev, A. M. *Sov. Physics Semiconductors-USSR* **1983**, *17*(9), 1027–1030.
(47) Heremans, J. P.; Jovovic, V.; Toberer, E. S.; Saramat, A.; Kurosaki, K.; Charoenphakdee, A.; Yamanaka, S.; Snyder, G. J. *Science* **2008**, *321*, 554.
(48) Ahmad, S.; Bilc, D.; Mahanti, S. D.; Kanatzidis, M. G. Ab Initio Studies Of Electronic Structure Of Defects In PbTe. *Proceedings of the Symposium On Semiconductor Defect Engineering-Materials Synthetic Structures And Devices Held At The 2005 MRS Spring Meeting*, San Francisco, CA, Mar 28−Apr 01, 2005; Ashok, S., Chevallier, J., Sopori, B. L., Tabe, M., Kiesel, P., Eds. San Francisco, CA, 2005; pp 455−460.
(49) Hoang, K.; Mahanti, S. D.; Jena, P. *Phys. Rev. B: Condens. Matter Mater. Phys*. **2007**, *76*(11), 115432/1–115432/18.
(50) Mahanti, S. D.; Hoang, K.; Ahmad, S. *Phys. B: Condens. Matter* **2007**, *401−402*, 291–295.
(51) Wei, S. H.; Zunger, A. *Phys. Rev. B* **1997**, *55*(20), 13605–13610.
(52) Larson, P.; Mahanti, S. D.; Kanatzidis, M. G. *Phys. Rev. B* **2000**, *61*(12), 8162–8171.
(53) Ono, T.; Irie, T.; Taahama, T. *J. Phys. Soc. Jpn*. **1962**, *17*(6), 1070–&.
(54) Rodot, H. *C. R. Hebdomadaires Des Seances De L Academie Des Sciences* **1959**, *249*(19), 1872–1874.
(55) Barabash, S. V.; Ozolins, V.; Wolverton, C. *Phys. Rev. B* **2008**, *78*(21), 214109.
(56) Barabash, S. V.; Ozolins, V.; Wolverton, C. *Phys. Rev. Lett*. **2008**, *101*, 155704.
(57) Hsu, K. F.; Loo, S.; Guo, F.; Chen, W.; Dyck, J. S.; Uher, C.; Hogan, T.; Polychroniadis, E. K.; Kanatzidis, M. G. *Science* **2004**, *303*, 818.
(58) Wang, H.; Li, J. F.; Nan, C. W.; Zhou, M.; Liu, W. S.; Zhang, B. P.; Kita, T. *Appl. Phys. Lett*. **2006**, *88*, 092104.
(59) Zhou, M.; Li, J.-F.; Kita, T. *J. Am. Chem. Soc*. **2008**, *130*(13), 4527–4532.
(60) Zhu, T. J.; Yan, F.; Zhang, S. N.; Zhao, X. B. *J. Phys. D: Appl. Phys*. **2007**, *40*(11), 3537–3540.
(61) Sugar, J. D.; Medlin, D. L. *J. Alloys Compd*. **2009**, *478*(1−2), 75–82.
(62) Quarez, E.; Hsu, K. F.; Pcionek, R.; Frangis, N.; Polychroniadis, E. K.; Kanatzidis, M. G. *J. Am. Chem. Soc*. **2005**, *127*, 9177.
(63) Cook, B. A.; Kramer, M. J.; Harringa, J. L.; Han, M. K.; Chung, D. Y.; Kanatzidis, M. G. *Adv. Funct. Mater*. **2009**, *19*(8), 1254–1259.
(64) Bilc, D. I.; Mahanti, S. D.; Kanatzidis, M. G. *Phys. Rev. B* **2006**, *74*(12), 125202.

(65) Androulakis, J.; Hsu, K. F.; Pcionek, R.; Kong, H.; Uher, C.; D'angelo, J. J.; Downey, A.; Hogan, T.; Kanatzidis, M. G. *Adv. Mater*. **2006**, *18*, 1170–1173.
(66) Poudeu, P. F. P.; D'angelo, J.; Downey, A. D.; Short, J. L.; Hogan, T.; Kanatzidis, M. G. *Angew. Chem., Int. Ed.* **2006**, *45*, 3835.
(67) Hoang, K.; Desai, K.; Mahanti, S. D. *Phys. Rev. B* **2005**, *72*, 064102.
(68) Gueguen, A.; Poudeu, P. F. P.; Li, C. P.; Moses, S.; Uher, C.; He, J. Q.; Dravid, V.; Paraskevopoulos, K. A.; Kanatzidis, M. G. *Chem. Mater*. **2009**, *21*(8), 1683–1694.
(69) Gueguen, A.; Poudeu, P. F. P.; Pcionek, R.; Kong, H.; Uher, C.; Kanatzidis, M. G. Thermoelectric Properties Of The Nanostructured $NaPb_{18-x}Sn_xMTe_{20}$ (M = Sb, Bi) Materials. *In Proceedings of the 8th Symposium On Themoelectric Power Generation Held at the 2007 MRS Fall Meeting*, Boston, MA, Nov 26−29, 2007; Hogan, T. P., Yang, J., Funahashi, R., Tritt, T. M., Eds.; Boston, MA, 2007; pp 349−354.
(70) Poudeu, P. F. P.; Guéguen, A.; Wu, C.-I.; Hogan, T.; Kanatzidis, M. G. Chem. Mater. **2009**, in press.
(71) Androulakis, J.; Lin, C. H.; Kong, H. J.; Uher, C.; Wu, C. I.; T, H.; Cook, B. A.; T, C.; Paraskevopoulos, M.; Kanatzidis, M. G. *J. Am. Chem. Soc*. **2007**, *129*, 9780.
(72) Lin, H.; Bozin, E. S.; Billinge, S. J. L.; Androulakis, J.; Malliakas, C. D.; Lin, C. H.; Kanatzidis, M. G. Phys. Rev. B **2009**, *80*, (4).
(73) Sootsman, J. R.; Pcionek, R. J.; Kong, H. J.; Uher, C.; Kanatzidis, M. G. *Chem. Mater*. **2006**, *18*(21), 4993–4995.
(74) Karkamkar, A. J.; Kanatzidis, M. G. *J. Am. Chem. Soc*. **2006**, *128*(18), 6002–6003.
(75) Arachchige, I. U.; Wu, J. S.; Dravid, V. P.; Kanatzidis, M. G. *Adv. Mater*. **2008**, *20*(19), 3638–+.
(76) Shah, P. S.; Husain, S.; Johnston, K. P.; Korgel, B. A. *J. Phys. Chem. B* **2001**, *105*(39), 9433–9440.
(77) Sooklal, K.; Hanus, L. H.; Ploehn, H. J.; Murphy, C. J. *Adv. Mater*. **1998**, *10*(14), 1083–+.
(78) Heremans, J. P.; Thrush, C. M.; Morelli, D. T. Phys. Rev. B **2004**, *70*, (11).
(79) Poudeu, P. F. P.; D'angelo, J.; Kong, H. J.; Short, J. L.; Pcionek, R.; Hogan, T.; Uher, C.; Kanatzidis, M. G. *J. Am. Chem. Soc*. **2006**, *128*, 14347.
(80) Kim, W.; Zide, J.; Gossard, A.; Klenov, D.; Stemmer, S.; Shakouri, A.; Majumdar, A. *Phys. Rev. Lett*. **2006**, *96*, 045901.
(81) Sootsman, J. R.; Kong, H.; Uher, C.; D'angelo, J. J.; Wu, C. I.; Hogan, T. P.; Caillat, T.; Kanatzidis, M. G. *Angew. Chem., Int. Ed.* **2008**, *47*(45), 8618–8622.
(82) Sootsman, J. R.; He, J. Q.; Dravid, V. P.; Li, C. P.; Uher, C.; Kanatzidis, M. G. *J. Appl. Phys*. **2009**, *105*, 083718.
(83) Hall, B. D.; Case, E. D.; Ren, F.; Johnson, J. R.; Timm, E. J. *Mater. Chem. Phys*. **2009**, *113*(1), 497–502.
(84) Hogan, T. P.; Downey, A.; Short, J.; D'angelo, J.; Wu, C. I.; Quarez, E.; Androulakis, J.; Poudeu, P. F. P.; Sootsman, J. R.; Chung, D. Y.; Kanatzidis, M. G.; Mahanti, S. D.; Timm, E. J.; Schock, H.; Ren, F.; Johnson, J.; Case, E. D. *J. Electron. Mater*. **2007**, *36*(7), 704–710.
(85) Pilchak, A. L.; Ren, F.; Case, E. D.; Timm, E. J.; Schock, H. J.; Wu, C. I.; Hogan, T. P. *Philos. Mag*. **2007**, *87*(29), 4567–4591.
(86) Ren, F.; Case, E. D.; Hall, B. D.; Ni, J. E.; Timm, E. J.; Wu, C. I.; D'angelo, J. J.; Hogan, T. P.; Lara-Curzio, E. *Philos. Mag. Lett*. **2009**, *89*(4), 267–275.
(87) Ren, F.; Case, E. D.; Ni, J. E.; Timm, E. J.; Lara-Curzio, E.; Trejo, R. M.; Lin, C. H.; Kanatzidis, M. G. *Philos. Mag*. **2009**, *89*(2), 143–167.
(88) Ren, F.; Case, E. D.; Sootsman, J. R.; Kanatzidis, M. G.; Kong, H. J.; Uher, C.; Lara-Curzio, E.; Trejo, R. M. *Acta Mater*. **2008**, *56*(20), 5954–5963.
(89) Ren, F.; Case, E. D.; Timm, E. J.; Jacobs, M. D.; Schock, H. J. *Philos. Mag. Lett*. **2006**, *86*(10), 673–682.
(90) Ren, F.; Case, E. D.; Timm, E. J.; Schock, H. J. *Philos. Mag*. **2007**, *87*(31), 4907–4934.
(91) Ren, F.; Case, E. D.; Timm, E. J.; Schock, H. J. *J. Alloys Compd*. **2008**, *455*(1−2), 340–345.
(92) Ren, F.; Hall, B. D.; Case, E. D.; Timm, E. J.; Trejo, R. M.; Meisner, R. A.; Lara-Curzio, E. *Philos. Mag*. **2009**, *89*(18), 1439–1455.
(93) Poudel, B.; Hao, Q.; Ma, Y.; Lan, Y. C.; Minnich, A.; Yu, B.; Yan, X.; Wang, D. Z.; Muto, A.; Vashaee, D.; Chen, X. Y.; Liu, J. M.; Dresselhaus, M. S.; Chen, G.; Ren, Z. *Science* **2008**, *320*, 634–638.
(94) Martin, J.; Nolas, G. S.; Zhang, W.; Chen, L. *Appl. Phys. Lett*. **2007**, *90*(22), 222112/1–222112/3.
(95) Ji, X.; Zhang, B.; Tritt, T. M.; Kolis, J. W.; Kumbhar, A. *J. Electron. Mater*. **2007**, *36*(7), 721–726.
(96) Tritt, T. M.; Zhang, B.; Gothard, N.; He, J.; Ji, X.; Thompson, D.; Kolis, J. W. Mater. Res. Soc. Symp. Proc. **2006**, *886* (Materials And Technologies For Direct Thermal-To-Electric Energy Conversion), 53−63.
(97) Ji, X.; He, J.; Alboni, P.; Su, Z.; Gothard, N.; Zhang, B.; Tritt, T. M.; Kolis, J. W. *Phys. Status Solidi R* **2007**, *1*(6), 229–231.
(98) Ji, X.; He, J.; Alboni, P. N.; Tritt, T. M.; Kolis, J. W. Mater. Res. Soc. Symp. Proc. **2008**, *1044*, Paper no. 1044-U01-02.
(99) Alboni, P. N.; Ji, X.; He, J.; Gothard, N.; Tritt, T. M. *J. Appl. Phys*. **2008**, *103*(11), 113707/1–113707/5.
(100) Li, H.; Tang, X. F.; Zhang, Q. J.; Uher, C. Appl. Phys. Lett. **2009**, *94*, (10).
(101) Ganesan, P. G.; Das, V. D. *Mater. Lett*. **2006**, *60*(17−18), 2059–2065.
(102) Martin, J.; Wang, L.; Chen, L.; Nolas, G. S. *Phys. Rev. B* **2009**, *79*, 115311.
(103) Wang, X. W.; Lee, H.; Lan, Y. C.; Zhu, G. H.; Joshi, G.; Wang, D. Z.; Yang, J.; Muto, A. J.; Tang, M. Y.; Klatsky, J.; Song, S.; Dresselhaus, M. S.; Chen, G.; Ren, Z. F. Appl. Phys. Lett. **2008**, *93*, (19).
(104) Bux, S. K.; Blair, R. G.; Gogna Pawan, K.; Lee, H.; Chen, G.; Dresselhaus, M. S.; Kaner, R. B.; Fleurial, J.-P. Adv. Funct. Mater. **2009**, *9999* (9999).
(105) Cahill, D. G.; Ford, W. K.; Goodson, K. E.; Mahan, G. D.; Majumdar, A.; Maris, H. J.; Merlin, R.; Phillpot, S. R. *J. Appl. Phys*. **2003**, *93*(2), 793–818.
(106) Li, D. Y.; Wu, Y. Y.; Kim, P.; Shi, L.; Yang, P. D.; Majumdar, A. *Appl. Phys. Lett*. **2003**, *83*(14), 2934–2936.
(107) Majumdar, A. *Science* **2004**, *303*, 777–778.
(108) Chen, G. *Semiconductors and Semimetals* **2001**, *71*, 203.
(109) Wang, Y.; Chen, X.; Cui, T.; Niu, Y. L.; Wang, Y. C.; Wang, M.; Ma, Y. M.; Zou, G. T. Phys. Rev. B **2007**, *76* (15).
(110) Popescu, A.; Woods, L. M.; Martin, J.; Nolas, G. S. Phys. Rev. B **2009**, *79* (20).
(111) Ren, F.; Case, E. D.; Sootsman, J. R.; Kanatzidis, M. G.; Kong, H.; Uher, C.; Lara-Curzio, E.; Trejo, R. M. *Acta Mater*. **2008**, *56*(20), 5954–5963.
(112) Gelbstein, Y.; Dashevsky, Z.; Dariel, M. P. *J. Appl. Phys*. **2008**, *104*(3), 033702/1–033702/4.
(113) Gelbstein, Y.; Gotesman, G.; Lishzinker, Y.; Dashevsky, Z.; Dariel, M. P. *Scr. Mater*. **2007**, *58*(4), 251–254.